NMR IN BIOMEDICINE
NMR Biomed. 2006; **19**: 300–315
Published online in Wiley InterScience (www.interscience.wiley.com). DOI:10.1002/nbm.1046

An introduction to coil array design for parallel MRI

Michael A. Ohliger* and Daniel K. Sodickson

Department of Radiology, and Department of Medicine, Cardiovascular Division, Beth Israel Deaconess Medical Center and Harvard Medical School, Boston, MA, USA; Harvard-MIT Division of Health Sciences and Technology, Boston, MA, USA

Received 22 November 2004; Revised 21 August 2005; Accepted 14 March 2006

ABSTRACT: The basic principles of radiofrequency coil array design for parallel MRI are described from both theoretical and practical perspectives. Because parallel MRI techniques rely on coil array sensitivities to provide spatial information about the sample, a careful choice of array design is essential. The concepts of coil array spatial encoding are first discussed from four qualitative perspectives. These qualitative descriptions include using coil arrays to emulate spatial harmonics, choosing coils with selective sensitivities to aliased pixels, using coil sensitivities with broad *k*-space reception profiles, and relying on detector coils to provide a set of generalized projections of the sample. This qualitative discussion is followed by a quantitative analysis of coil arrays, which is discussed in terms of the baseline SNR of the received images as well as the noise amplifications (*g*-factor) in the reconstructed data. The complications encountered during the experimental evaluation of coil array SNR are discussed, and solutions are proposed. A series of specific array designs are reviewed, with an emphasis on the general design considerations that motivate each approach. Finally, a set of special topics is discussed, which reflect issues that have become important, especially as arrays are being designed for more high-performance applications of parallel MRI. These topics include concerns about the depth penetration of arrays composed of small elements, the use of adaptive arrays for systems with limited receiver channels, the management of inductive coupling between array elements, and special considerations required at high field strengths. The fundamental limits of spatial encoding using coil arrays are discussed, with a primary emphasis on how the determination of these limits impacts the design of optimized arrays. This review is intended to provide insight into how arrays are currently used for parallel MRI and to place into context the new innovations that are to come. Copyright © 2006 John Wiley & Sons, Ltd.

KEYWORDS: parallel MRI; coil array; radiofrequency coil; SNR; sensitivity; SENSE; SMASH; coil design

INTRODUCTION

Parallel MRI techniques accelerate image acquisitions by extracting spatial information from the sensitivity patterns of radiofrequency (RF) coil arrays and using that information to substitute for a portion of the data that would normally be acquired using sequentially applied magnetic field gradients. In recent years, these strategies have been embraced clinically and exploited in order to increase patient comfort, enhance spatial resolution, expand anatomical coverage and reduce image artifacts. While the detailed mechanics of the various procedures for image reconstruction are dealt with in other articles within this special issue, it should be clear that the effectiveness of any parallel reconstruction technique is fundamentally limited by the amount of spatial information contained within a coil array. Therefore, a careful choice of coil array design is critical for the effective use of parallel MRI. This review is intended to provide a comprehensive introduction to the basic principles of coil array design for parallel MRI.

Even when accelerated imaging is not required, detector arrays are ubiquitous tools in MRI because they provide images with a high signal-to-noise ratio (SNR) across a large field of view (1). This SNR advantage arises because each detector in an array responds to magnetization from local regions, while ignoring magnetization (and noise) from the rest of the sample. Parallel MRI methods similarly take advantage of the local nature of each coil's reception pattern in order to extract additional spatial information about the sample.

The use of coil arrays for spatial encoding has led to new design considerations. One manifestation of these new considerations has been an expansion of the number of coil elements found in a typical array. When parallel MRI techniques were first introduced, the majority of clinical MRI scanners were able to acquire data simultaneously from either four or six detector coils. The restrictions on the number of independent detectors that could be incorporated into an array not only limited the maximum theoretical

**Correspondence to:* M. A. Ohliger, 330 Brookline Ave, AN 235, Beth Israel Deaconess Medical Center, Boston, MA 02215, USA.
E-mail: Mohliger@mit.edu
Contract/grant sponsor: NIH; *contract/grant numbers:* R29 HL60802; R01 EB000447; R01 EB002568.

Abbreviations used: FOV, field of view; *g*-factor, geometry factor; MR, magnetic resonance; MRI, magnetic resonance imaging; PILS, partially parallel imaging with localized sensitivities; RF, radio frequency; ROI, region of interest; SAR, specific absorbtion rate; SMASH, simultaneous acquisition of spatial harmonics; SNR, signal-to-noise ratio; SENSE, sensitivity encoding; TEM, transmit electromagnetic.

image acceleration to either 4- or 6-fold, but these restrictions also led to a degradation of image quality even for more modestly accelerated images. Early investigators used time-domain multiplexing to incorporate an eight-element coil array into a single-channel MR system (2). Largely as a result of developments in parallel MRI, MR systems with eight or more independent receiver channels have become routinely available. Prototype MR scanners have been introduced with 16 (3), 32 (4–7) and 64 (8) receiver channels, and commercial systems with 32 channels are also now available.

Accompanying this expansion in the number of available receiver channels on many systems, there has been a remarkable diversity in the coil arrays that have been created specifically for parallel MRI. In an effort to tailor coil arrays' spatial encoding properties, researchers have sought new ways of customizing the sensitivity profiles of individual detectors, and they have also explored novel geometrical arrangements for those coil array elements. The present review is not intended as an enumeration of all of the coil arrays that have been proposed for parallel MRI to date, nor does it presume to make pronouncements about 'good' or 'bad' design ideas. Rather, a group of formal and intuitive tools are introduced that coil array designers can apply to new design approaches.

The next section begins with a brief review of the basic parallel MRI formalism, which provides a conceptual and notational foundation for the rest of the article. Section 3 is devoted to a qualitative discussion of what we mean when we say that a coil array does (or does not) provide spatial information about a sample. This qualitative discussion serves as a starting point for exploring new array designs. Section 4 discusses various ways that coil arrays are evaluated quantitatively, and Section 5 provides concrete examples of several approaches to coil array design that have been explored to date. Finally, Section 6 describes several special topics that are of current interest in parallel MRI.

BASIC CONCEPTS

Parallel MRI formalism

While a detailed discussion of the various parallel MRI reconstruction techniques is beyond the scope of this article, it is necessary to review a number of basic concepts in order to establish the formalism and terminology that is used in subsequent sections. In a general parallel MRI reconstruction (9,10), the MR signal received from coil l at k-space position, $\mathbf{k}_m$, in response to precessing transverse magnetization that has density, $M(\mathbf{r})$, is discretized and written as

$$S_l(\mathbf{k}_m) = \sum_{\text{voxel}\, j} C_l(\mathbf{r}_j) M(\mathbf{r}_j) \mathrm{e}^{i\mathbf{k}_m \cdot \mathbf{r}_j} + n_l(\mathbf{k}_m) \qquad (1)$$

In this equation, $C_l(\mathbf{r}_j)$ represents the spatial sensitivity pattern of each detector, and $n_l(\mathbf{k}_m)$ is the noise that is recorded along with the signal from each k-space point. If the acquired signal and noise, together with the magnetization density, are written as column vectors, then the signal equation becomes

$$\mathbf{S} = \mathbf{EM} + \mathbf{n} \qquad (2)$$

where the encoding matrix, $\mathbf{E}$, is given by

$$E_{(lm),j} \equiv C_l(\mathbf{r}_j) \mathrm{e}^{i\mathbf{k}_m \cdot \mathbf{r}_j} \qquad (3)$$

Within this formalism, reconstructing an image amounts to finding a matrix, $\mathbf{F}$, such that $\mathbf{FE}$ is equal to the identity matrix. In general, $\mathbf{E}$ is a rectangular matrix, and there are many possible choices for $\mathbf{F}$. It has been shown (9,10) that the minimum-norm solution of eqn (2), which leads to a reconstructed image with the least possible noise, is given by

$$\mathbf{F}_{\text{min norm}} = (\mathbf{E}^\dagger \Psi^{-1} \mathbf{E})^{-1} \mathbf{E}^\dagger \Psi^{-1} \qquad (4)$$

Here, Ψ is the coil array's noise covariance matrix, which describes the noise statistics of the various coils. Formally, Ψ can be written as

$$\Psi \equiv \left\langle (\mathbf{n} - \overline{\mathbf{n}})(\mathbf{n} - \overline{\mathbf{n}})^\dagger \right\rangle_{\text{time}} \qquad (5)$$

where the angled brackets indicate a temporal average and $\overline{\mathbf{n}}$ is a vector containing the time-average of each noise channel (for white noise, this is generally zero). We can also define a noise *correlation* matrix, which is a normalized version of Ψ:

$$\Psi_{ij}^{\text{corr}} \equiv \frac{\Psi_{ij}}{\sqrt{\Psi_{ii}\Psi_{jj}}} \qquad (6)$$

The noise correlation matrix is useful because it represents intrinsic correlations between the noise signals of various coils, and it is independent of the overall amplifier gain in each channel. It is important to note, however, that for the purposes of image reconstruction [eqn (4)], the unnormalized noise covariance matrix is the relevant quantity.

Because noise from separately acquired points in k-space is generally independent, Ψ is block-diagonal. The diagonal elements of Ψ are equal to the total noise power received by a given coil, and the off-diagonal elements of Ψ represent correlations in noise between multiple coils. The mere presence of correlated noise does not, by itself, reflect poorly on a given coil array. In fact, for any array with a non-singular noise covariance matrix, a linear transformation may always be found such that the noise from all of the combined channels is uncorellated (11). The predominant criterion for judging a coil array is the SNR of the final image, which will be discussed in a later section.

QUALITATIVE DESCRIPTIONS OF SPATIAL ENCODING USING COIL ARRAYS

The design and construction of coil arrays for conventionally gradient-encoded applications of MRI has

been extensively discussed elsewhere (1,12). In this article, we focus mainly on those design considerations that are unique to coil arrays that are used with parallel MRI. The most important design principle for parallel MRI detectors is based on the recognition that, while gradient-induced spatial harmonic functions are orthogonal to each other over a chosen field-of-view, the sensitivity-modulated harmonics [$C_l(\mathbf{r})\exp(i\mathbf{k}_m \cdot \mathbf{r})$, also called 'encoding functions'] generally are not orthogonal. This lack of orthogonality is responsible for amplified noise in the final reconstructed image, and an analysis of these noise amplifications forms the basis for most quantitative assessments of array performance. Before discussing these quantitative tools in more detail, we describe a number of qualitative ways of viewing the spatial information that detector arrays provide in parallel MRI. Many of these qualitative descriptions are derived from specific algorithms that have been developed to reconstruct parallel MRI data. While each perspective on spatial encoding that is presented here is, at some level, equivalent, each perspective is still valuable for the unique insights that it is able to provide.

Emulation of spatial harmonics

Coil arrays can provide spatial information about a sample by emulating the spatial modulations produced by the magnetic field gradients that have been omitted from the acquisition. This idea is the basis of the SMASH technique (13). Specifically, if a set of coefficients are found such that

$$\sum_{l=1}^{N} w_l C_l(\mathbf{r}) = \mathrm{e}^{i\Delta\mathbf{k}\cdot\mathbf{r}} \tag{7}$$

the same linear combination can be applied to the acquired MR data

$$\begin{aligned}\sum_{l=1}^{N} w_l S_l(\mathbf{k}) &= \int_{\text{sample}} \left(\sum_{l=1}^{N} w_l C_l(\mathbf{r})\right) M(\mathbf{r})\exp(i\mathbf{k}\cdot\mathbf{r})d^3\mathbf{r} \\ &= S(\mathbf{k}+\Delta\mathbf{k})\end{aligned} \tag{8}$$

The effect of applying the coefficients, w_l, is to 'move' the acquired data in k-space by a distance $\Delta\mathbf{k}$.

The accuracy of the reconstructed line $S(\mathbf{k}+\Delta\mathbf{k})$ depends on the accuracy of the linear fit in eqn (7). From this perspective, one approach to designing coil arrays is to choose detectors that have linear combinations that approximate spatial harmonics as accurately as possible. This procedure is described schematically in Fig. 1(a) for a coil array with three component coils. In this example, the array is placed 8 cm above a coronal image plane. The top panel of the figure shows the magnitude of the coil sensitivities calculated along the central frequency-encode line. The bottom panel shows how the coil sensitivities may be combined to approximate the real and imaginary components of the first spatial harmonic. As an alternative to linear combinations of coil sensitivities, a single coil with a harmonic sensitivity profile can also be used within this approach to spatial encoding (14–16). Coils with harmonic profiles will be discussed further later.

Unfolding of aliased data

When data are acquired on a Cartesian k-space grid and then undersampled by a factor, R, the reconstructed image is aliased. Each reconstructed pixel represents the sum of R equally spaced voxels across the field-of-view,

$$S_l(x_0) = \sum_{j=1}^{R} C_l(x_0 + j\Delta x)M(x_0 + j\Delta x) \tag{9}$$

where $\Delta x = \mathrm{FOV}/R$. The process of aliasing is shown schematically in Fig. 1(b), where two pixels from each of the three component coil images (top row) are folded into a single pixel within the aliased images (bottom row). It is possible to reconstruct a fully sampled image from the aliased data because each coil is predominantly sensitive to one or the other aliased pixel. In the most extreme case [which is *not* the case in Fig. 1(b)], if the sensitivity for coil l is large at a point x_0 and small at the aliased points $x_0 + j\Delta x$, then the signal from coil l will principally represent the magnetization at x_0 and not at the aliased points:

$$S_l(x_0) \approx C_l(x_0)M(x_0) \tag{10}$$

The partially parallel imaging with localized sensitivities (PILS) reconstruction technique (17) is based on the assumption of completely localized coil sensitivities. The Subencoding reconstruction technique (18,19) as well as the image-domain formulation of SENSE (9) operate using a similar principle, but allow for situations such as in Fig. 1(b), where the coil sensitivities are incompletely localized.

When the parallel MRI reconstruction is viewed as the unfolding of aliased pixels, it is clear that coil arrays with component coil sensitivities that are spatially selective for different aliased regions will be effective at reconstructing undersampled data. Aliased regions of a sample may also be resolved by employing coils that have different phase variations across the sample. For example, it has been shown while a loop coil and a butterfly coil have similar magnitude profiles, their distinct phase variations are still sufficient to allow them to unfold aliased data (20). The importance of coil phase to image reconstructions will be discussed later in the context of specific coil design approaches.

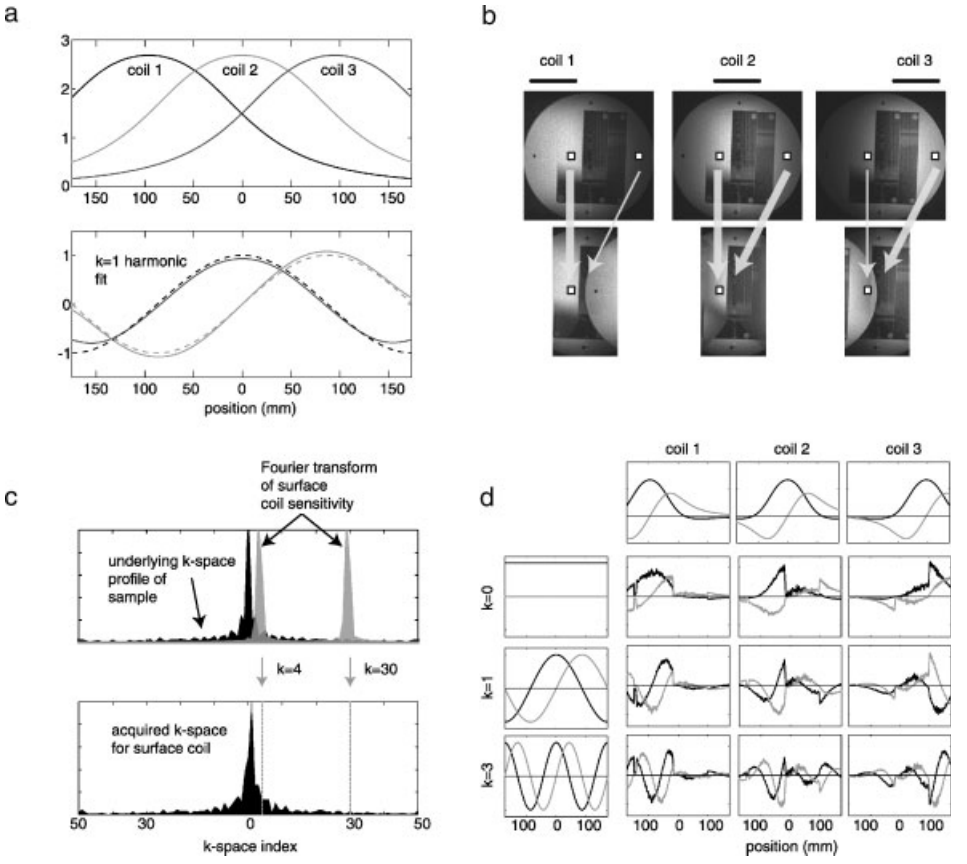

Figure 1. Schematic illustrations of several qualitative perspectives on coil array spatial encoding. Each illustration was generated by simulating a three-coil array located 8 cm above a coronal image plane. (a) The magnitude coil sensitivities along the central frequency-encode line are shown in the top plot. The bottom plot illustrates the least-squares fits (solid lines) of the real (black) and imaginary (gray) parts of the coil sensitivities to the first spatial harmonic on the FOV (dashed lines). (b) Three simulated component-coil images (top row) are undersampled to generate three aliased images (bottom row). Two pixels in the fully encoded images fold onto a single pixel in the aliased images. Spatial information is available because each component coil sees the two aliased pixels with different relative signal intensities (indicated by the widths of the arrows). (c) Convolution of the sample's underlying *k*-space distribution (top graph, black curve) by a single component coil's spatial frequency response function (gray curves). In this figure, the convolution process is explicitly shown at the $k=4$ and $k=30$ lines. Each point in the acquired component coil *k*-space (bottom curve) is a weighted sum of several surrounding frequency components from the sample magnetization. (d) Each acquired *k*-space point from each component coil gives a generalized projection through the sample, which is known as an encoding function. The real (dark curves) and imaginary (light curves) parts of nine example projections through the central line of simulated sample are shown.

Broadening of the acquired *k*-space data

The Fourier transform of the product $C(\mathbf{r})M(\mathbf{r})$ in the MR signal equation for a given coil l can be written as the convolution of the two functions' Fourier transforms, $\tilde{C}(\mathbf{k})$ and $\tilde{M}(\mathbf{k})$:

$$S_l(\mathbf{k}) = \int \tilde{C}_l(\mathbf{k}')\tilde{M}(\mathbf{k}-\mathbf{k}')d^3\mathbf{k}' \qquad (11)$$

This process is shown graphically in Fig. 1(c) for one coil element within a three-coil array. Because of the convolution by the coil array frequency-response function, each spectral component of the surface coil data contains information about several surrounding spatial frequencies within the sample magnetization. As a consequence, the widths of the component coils' spatial frequency spectra set an upper bound on the distance that is allowed between the acquired *k*-space points and the missing *k*-space points that need to be reconstructed (21). Of course, regardless of how broad each individual sensitivity pattern is in *k*-space, the signals from several coils (each with different *k*-space profiles) must still be combined to reconstruct images correctly. Several

parallel imaging techniques (10,22,23) exploit the limited spatial frequency content of coil sensitivities in order to simplify the reconstruction of undersampled data.

Generalized spatial projections

The formal grouping of coil sensitivities together with the sinusoidal modulations induced by the gradients into an encoding matrix [eqn (3)] suggests that each acquired piece of data is a 'generalized projection' through the sample (10). Examples of these projections for a three-coil array are plotted in Fig. 1(d). Coil array sensitivities can be tailored for parallel imaging such that they lead to overall projection functions that are as spatially orthogonal as possible. This perspective on spatial encoding is particularly powerful because it is easily adapted to various encoding schemes. Indeed, while much focus is placed on designing coil sensitivities to complement the gradient-encoded Fourier harmonics, it should also be possible to implement non-Fourier gradient encoding techniques that complement the coil sensitivities.

QUANTITATIVE ANALYSIS OF ARRAY PERFORMANCE

SNR behavior of parallel MRI

The previous section discussed a number of qualitative perspectives on coil array spatial encoding. This section discusses the theoretical and experimental tools that are used to evaluate coil arrays quantitatively. These quantitative tools are key to refining particular design approaches and they also provide an objective basis for comparing arrays.

As mentioned earlier, one of the chief distinctions between parallel MRI and fully gradient-encoded Fourier imaging is that the encoding functions used for parallel imaging [eqn (3)] are generally not spatially orthogonal. As a consequence, the reconstruction matrix [eqn (3)] is typically not unitary, and there is a spatially varying increase in noise throughout the image (9,24). The total amount of noise amplification that is introduced by the reconstruction is strongly dependent on the choice of array design. Because the image reconstruction used in eq. (4) is a linear transformation, the noise power of an R-fold accelerated reconstruction can be calculated from the encoding matrix (9),

$$(\sigma_j^R)^2 \propto [(\mathbf{E}_R^\dagger \Psi^{-1} \mathbf{E}_R)^{-1}]_{j,j} \qquad (12)$$

where $\mathbf{E}_R$ is the encoding matrix corresponding to an R-fold accelerated acquisition. Using the same array in the absence of parallel imaging, the encoding matrix is $\mathbf{E}_{\text{full}}$ and the noise power is given by

$$(\sigma_j^{\text{FULL}})^2 \propto [(\mathbf{E}_{\text{full}}^\dagger \Psi^{-1} \mathbf{E}_{\text{full}})^{-1}]_{j,j} \qquad (13)$$

Therefore, the change in SNR that occurs as a consequence of parallel imaging can be written formally as

$$\left(\frac{\text{SNR}_j^R}{\text{SNR}_j^{\text{FULL}}}\right)^2 = \left(\frac{\sigma_j^{\text{FULL}}}{\sigma_j^R}\right)^2 = \frac{[(\mathbf{E}_{\text{full}}^\dagger \Psi^{-1} \mathbf{E}_{\text{full}})^{-1}]_{j,j}}{[(\mathbf{E}_{\text{R}}^\dagger \Psi^{-1} \mathbf{E}_{\text{R}})^{-1}]_{j,j}}. \qquad (14)$$

Geometry factor

In the special case of an image with uniform Cartesian sampling, eqn (14) can be written in the compact form (9):

$$\text{SNR}^R = \frac{\text{SNR}^{\text{FULL}}}{\sqrt{R[(\mathbf{E}_R^\dagger \Psi^{-1} \mathbf{E}_R)]_{j,j}[(\mathbf{E}_R^\dagger \Psi^{-1} \mathbf{E}_R)^{-1}]_{j,j}}} \qquad (15)$$

The factor of $\sqrt{R}$ in the denominator of eqn (15) reflects the fact that, for Fourier sampling, $[\mathbf{E}_{\text{full}}^\dagger \Psi^{-1} \mathbf{E}_{\text{full}}]_{j,j} = R[(\mathbf{E}_{\text{R}}^\dagger \Psi^{-1} \mathbf{E}_{\text{R}})]_{j,j}$. This factor represents an overall loss in SNR that occurs simply because there are fewer acquired k-space points. Changes in coil array design have very little impact on this effect. The second term in eqn (15) describes a spatially dependent amplification of noise, which has become known as the geometry factor, or 'g-factor:'

$$g_j \equiv \sqrt{[(\mathbf{E}_R^\dagger \Psi^{-1} \mathbf{E}_R)]_{j,j}[(\mathbf{E}_R^\dagger \Psi^{-1} \mathbf{E}_R)^{-1}]_{j,j}} \qquad (16)$$

The g-factor is (by definition) always greater than or equal to one, and it quantifies the fractional loss in SNR that occurs due to the non-orthogonality of the array coil sensitivities. While the compact expression for the g-factor in eqn (16) applies strictly to images with uniform Cartesian k-space sampling patterns, the more general expression in eqn (14) can still be used for arbitrary sampling patterns.

The g-factor profile for a simulated three-coil array that is located 8 cm above a coronal image plane is shown in Fig. 2. The locations of the coil array elements are shown in the top portion of the figure. The g-factor plot shown below the array corresponds to the reconstruction of 3-fold undersampled data. For clarity, the plot shown is restricted to the central set of frequency-encode lines. Because the undersampling factor is equal to the number of coils in the array, it is not surprising that there are large peaks of noise amplification within the FOV. In order to visualize these noise amplifications, noise has been added to simulated component-coil images. These images were

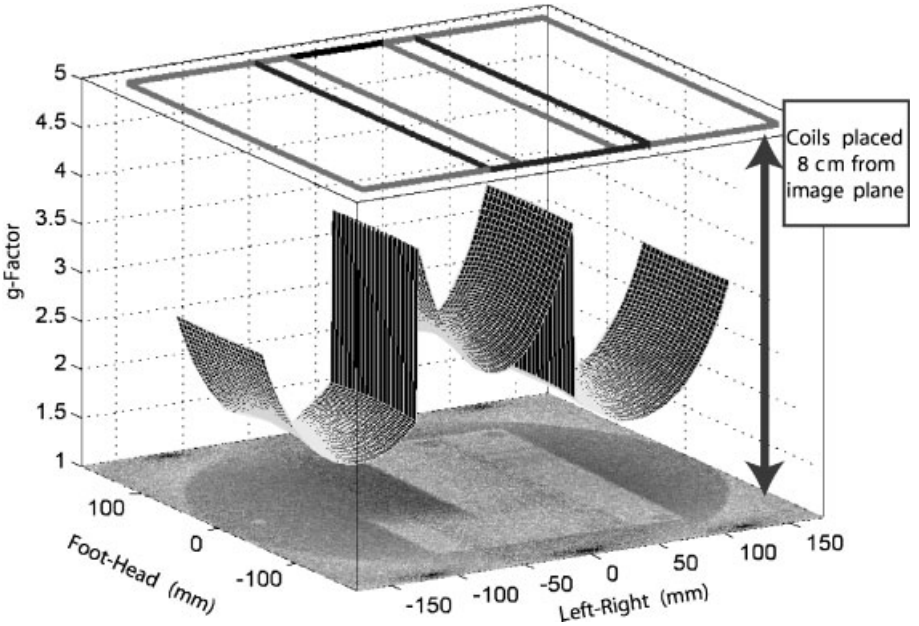

Figure 2. Geometry factor for a simulated 3-coil rectangular array (shown at the top of the image) viewing a coronal sample plane that is 8 cm below the array. The sample FOV is 35 cm along each dimension and the acceleration factor is 3. The surface plot shows the *g*-factor for the central frequency-encode lines as a function of spatial position. The bottom image is reconstructed following the injection of sample noise to the simulated component coil data.

undersampled by a factor of 3, and then reconstructed using a SENSE reconstruction. The noise clearly increases in those regions where the *g*-factor plot is high. While the *g*-factor plot in Fig. 2 appears to be highest directly below the places where the coil elements overlap, this is not a universal characteristic of such plots. Indeed, the reconstruction of 2-fold undersampled data with the same simulated coil array and geometrical configuration yields peaks in *g*-factor that are directly below the central coil and at the edges of the FOV (results not shown). This underscores the need to investigate each coil array for the particular imaging situation that is desired.

When evaluating coil arrays for image reconstructions other than SENSE, it is straightforward to derive an analytical formula for the geometry-related SNR changes that is analogous to eqn (14), as long as the overall reconstruction procedure represents a linear transformation. Analytical SNR formulas are more complicated, however, for reconstructions that involve nonlinear transformations such as sum-of-squares coil combinations (23,25–27). An alternative method for predicting the SNR effects of using a particular coil array in a parallel reconstruction involves adding simulated noise to a sample image, and measuring the pixel-by-pixel SNR of the reconstructed data (28) (see the cautionary points regarding SNR measurement below). This approach was also followed in the SNR analysis of Ref. (26). This simulation-based technique is particularly valuable for parallel reconstruction methods for which analytic SNR formulations are cumbersome, or for reconstructions that require iterative matrix inversions.

Because many of the sequence-dependent determinants of SNR have been removed from the expression for the *g*-factor in eqn (16), this parameter has become an attractive figure of merit for assessing the performance of coil arrays for parallel MRI. While the *g*-factor is a generally useful measure, it does have several limitations. For example, changes in coil geometry will likely alter a coil array's baseline SNR [eqn (13)], together with that array's *g*-factor. Naturally, improvements in *g*-factor are not valuable when they come at the cost of severe degradations in the overall performance of an array. In addition, the *g*-factor is a function of *both* the coil sensitivities and the pattern of acquired *k*-space lines. Therefore, the *g*-factor will, in general, be different for different undersampling factors, object sizes and image planes. Finally, it is important to recognize that while the *g*-factor is predominantly dependent on the acquisition pattern and the coil sensitivities, there is still a second-order dependence of *g* on the noise covariance matrix, $\mathbf{\Psi}$. Drastic changes in an array's baseline noise power can also affect the array's *g*-factor.

Computational array analysis

Equations (14)–(16) are analytical tools for evaluating coil array performance for parallel MRI. In order to make use of these expressions, it is necessary to know (1) the

coil sensitivities, $C_l(\mathbf{r})$, (2) the noise covariance matrix, $\mathbf{\Psi}$, and (3) the pattern of the *k*-space acquisition. The *k*-space acquisition pattern is determined by the desired image plane geometry and pulse sequence. The coil sensitivities and noise covariance matrix can, of course, be measured empirically at the time of imaging. However, for understanding and designing coil arrays, it is useful to have methods for predicting $C_l(\mathbf{r})$ and $\mathbf{\Psi}$ computationally.

The spatial sensitivity pattern, $C_l(\mathbf{r})$, of each coil within an array can be calculated using the well-known principle of reciprocity (29–32). The principle of reciprocity states that the magnetic flux induced through a coil by precessing magnetization can be written in terms of $\hat{\mathbf{B}}^{\text{coil}}$, which is the magnetic field that would be generated by a unit current flowing around that coil. Accordingly, the complex spatial sensitivity function can be written in terms of the two transverse components of $\hat{\mathbf{B}}^{\text{coil}}$,

$$C_l(\mathbf{r}) = [\hat{B}_x^{\text{coil}}(\mathbf{r})]_l - i[\hat{B}_y^{\text{coil}}(\mathbf{r})]_l \qquad (17)$$

The noise covariance matrix can similarly be computed in terms of $\hat{\mathbf{E}}^{\text{coil}}$, which is the electric field created by a unit current flowing around the conductor path of the coil (1,33,34):

$$\Psi_{ll'} = 4kT\Delta f \int \sigma(\mathbf{r})\hat{\mathbf{E}}_l(\mathbf{r}) \cdot \hat{\mathbf{E}}_{l'}^*(\mathbf{r})d^3\mathbf{r} \qquad (18)$$

In this expression, $\sigma(\mathbf{r})$ is the sample conductivity, T is the absolute temperature, k is Boltzmann's constant, and Δf is the receiver bandwidth.

The field definitions of $C_l(\mathbf{r})$ and $\mathbf{\Psi}$ permit the theoretical evaluation of any prospective coil array design. Systematic and detailed coil array design examples that illustrate these principles have been presented for cardiac (35) as well as for head (36,37) imaging.

Experimental analysis of array performance

As described in the previous sections, the major criteria for evaluating coil array performance for parallel MRI are based on the SNR of the reconstructed images. However, measuring the SNR of an image that has been reconstructed using parallel MRI is significantly more complicated than it is for images that have been fully acquired using gradient-encoding. Traditionally, the image SNR in MRI is measured by choosing two regions of interest: one region inside the sample, and one region in the background noise. The mean of the region within the sample is used as the signal and the standard deviation of the region outside of the sample is used as an estimate of the noise.

This traditional approach to measuring SNR is problematic in the context of parallel MRI for two reasons. The first reason is related to the use of magnitude data, rather than complex image pixels. The magnitude operation is nonlinear, and it introduces a bias into regions of the image that have low SNR. Even without using parallel MRI, this noise bias can introduce measurement errors (38). The SNR analysis of magnitude reconstructions becomes even more challenging when parallel MRI reconstructions are used because in parallel reconstructions, the SNR for every pixel (and thus the noise bias) is generally different (27). Because of these complications, it is nearly always advisable to perform SNR analyses on complex-valued images.

The second difficulty encountered when measuring the SNR of a parallel MRI-reconstructed image occurs even when complex-valued data are used for the measurement. Because the *g*-factor varies spatially, a noise estimate taken in one region (e.g. outside of the sample) is not reflective of the noise in other regions (see Fig. 2). Furthermore, the noise between pixels in parallel MRI is generally correlated (9) (although, to be fair, the noise is typically not correlated between *adjacent* pixels), and the statistical analysis of an ROI does not reliably correspond to an equivalent temporal sampling. Finally, many implementations of parallel MRI perform a masking or other nonlinear operation on regions outside of the sample, which can further complicate noise measurements from those regions.

With these complications in mind, we discuss two practical approaches to evaluating the SNR of parallel MRI data. The first method is used in Refs (35,36), and is based on the theoretical noise analysis for SENSE described above. If the noise covariance matrix, Ψ, and the coil sensitivities, $C_l(\mathbf{r})$, of the array have been measured, then eqn (13) can be used to calculate the noise power in each reconstructed pixel, and eqn (16) can be used to calculate the *g*-factor of each pixel. The ratio of the signal to the noise power in each pixel gives the SNR in each pixel, and then an average SNR over the entire region can be reported. The advantage of this approach is that it is simple to implement and readily applicable to *in vivo* acquisitions. The disadvantage is that the SNR of the image is, in some sense, being calculated from a theoretical model and not measured.

An alternative approach to SNR analysis involves the use of an imaging phantom (39,40). A repeated set of undersampled acquisitions is performed and reconstructed using a parallel MRI technique of choice. The mean and standard deviation over the set of replicas for each (complex-valued) pixel in the image is measured, creating an SNR map. The average values over different regions of the SNR map are then reported. Because of the number of repetitions involved, this approach is not practical for *in vivo* imaging. Furthermore, in this approach, both thermal noise and intrinsic system instabilities will contribute to the measured noise. The long-term system instabilities might have various causes, including variations in the RF transmitter power or

temperature changes in the components that make up the receiver circuitry. The relative contributions of system instabilities to the measured noise (compared to thermal noise) can be minimized by using pulse sequences with relatively low baseline SNR. Some balance is necessary when using this strategy, because if the SNR is too low, more samples will be required to measure each pixel's mean and standard deviation. The resulting increase in scan time may potentially increase the influence of the long-term system variations.

SPECIFIC DESIGN EXAMPLES

In this section, a number of concrete array design examples are reviewed. It is not practical for us to present every specific coil array that has been proposed for parallel MRI to date. Instead, a series of broad categories are described that help to establish a systematic framework for understanding the wide range of array designs that have been presented in the literature. Each design approach highlights one or more degrees of freedom that are available to coil designers when developing a new coil array. For reference, Fig. 3 contains schematic diagrams illustrating the geometries of several arrays that are discussed in this section.

RF coil arrays may be broadly categorized in two ways. The first categorization is based on the types of detectors that make up the individual array elements. Nearly every type of resonant structure available in conventional MRI has been applied to parallel imaging. Each type of array element offers its own opportunities for tailoring the detector's reception sensitivity in order to achieve the best possible SNR and geometry factor. The second categorization for coil arrays is based on the geometric arrangement of the detectors. The array designs discussed here are presented as geometrical variations of a few basic detector types. This organization has been chosen because it offers a relatively smooth progression from more basic coil array types into more advanced design concepts.

Simple loop surface coils

One of the most straightforward coil array design approaches is based on surface coils that are made of simple conducting loops. We begin by considering a set of small loop coils that are tiled together to cover an entire FOV. Broadly speaking, these coils can be arranged in straight lines, two-dimensional grids, or wrap-around arrays that surround the sample axially. One of the basic principles of coil array design for parallel MRI is that coil elements should be arranged so that they have sensitivity variations that are principally aligned with the direction of undersampling. From the perspective of emulating spatial harmonics, elements must be aligned so that they can reproduce the missing *k*-space lines. From the perspective of resolving aliased pixels, coils must be located so that they can be sensitive to different aliased regions of the image.

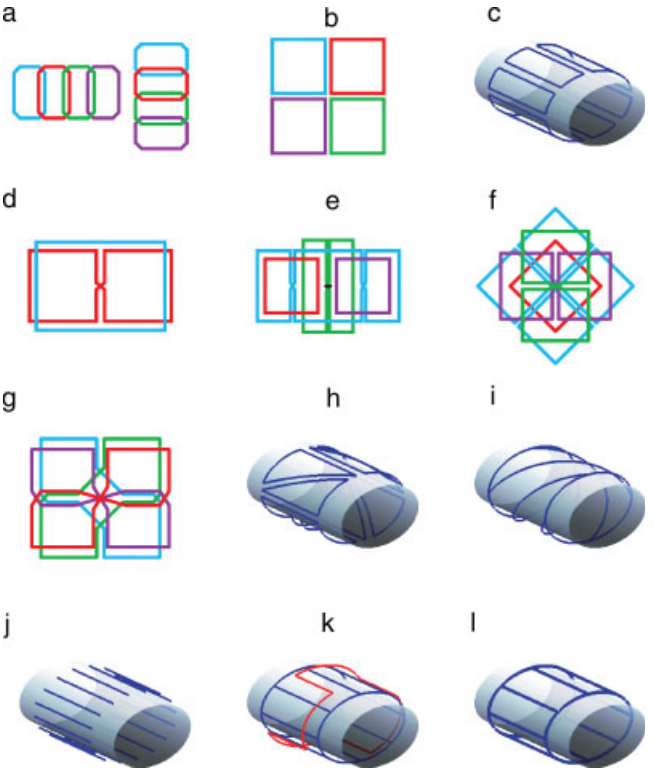

Figure 3. Schematic illustration of several coil array described in this text. Only the major geometrical features of each coil array are depicted, and the element numbers and coil dimensions may not exactly match those of the cited references. (a) Linear arrays of loop coils; (b) 2×2 grid of loop coils. (c) 'Wrap-around' arrangement of eight loop coils. (d) Quadrature pair of butterfly and loop coils (20). (e) 'Saddle-train' coil (45); red and purple elements are simple loops, green element is a single butterfly, and blue element is a double-twisted saddle train coil. (f) 'Concentric' coil array (49,50); the red coil is a simple loop, green and purple elements are two-lobed butterfly coils in perpendicular orientations, the blue coil is a four-lobed cloverleaf element. (g) 'Diagonal' coil array (51); blue and green coils are top logically simple loops in diagonal orientations; red and purple elements are crossed saddle elements, also in diagonal orientations. (h) Triangular coil array (53,111), with eight right-triangular elements. (i) Spiral birdcage coil (16,55). (j) TEM-resonator arrays. (k) Degenerate-mode birdcage coil (66). Red conductor is used to simultaneously resonate the uniform and gradient modes. (l) Birdcage coil designed to produce spatial harmonic sensitivities (15) (details of conductors not shown).

For a fixed number of array elements, linear arrays (2,17) [Fig. 3(a)] provide for the maximum amount of spatial information in a single direction. Grid-type arrays (4,41) [Fig. 3(b)] and wrap-around arrays (36,37) [Fig. 3(c)] provide fewer elements in any specific direction, but their multidimensional characters allow for simultaneous undersampling in several directions at once. The ability to encode spatial information in multiple

directions is important for several reasons. First, many imaging protocols require the acquisition of multiple studies with different image plane orientations, and it is clearly not desirable to use a different coil array every time the image plane orientation changes. Furthermore, there are applications such as cardiac imaging where oblique image planes are chosen to match the patient's anatomy, and it is impossible to predict the exact image plane orientation beforehand. Finally, it has been shown that simultaneous undersampling along two (or more) dimensions at once leads to a smaller geometry factor than would an equivalent amount of net acceleration along one dimension (42,43). Alternative approaches to multidimensional encoding, which complement the grid and wrap-around arrays described here, will be discussed in a later section.

The preceding discussion highlights one of the most significant differences between coil array design for parallel MRI and coil array design for conventional gradient-encoded MRI. In conventional gradient-encoded MRI, coil array design is largely independent of the choice of acquisition strategy. In parallel MRI, on the other hand, the direction of sensitivity variation needs to be carefully coordinated with the direction of *k*-space undersampling.

Surface coils with complex looping structures, the importance of coil phase

One common attribute of the simple loop-based array designs discussed above is that spatial encoding is largely accomplished by having surface coil sensitivities with varying magnitudes across the field of view. Of course, because coil sensitivities are complex-valued functions of position, it is implicit in the parallel MRI reconstruction algorithm, eqn (4), that the phases of the coil sensitivities are just as important for spatial encoding as are the magnitudes. As mentioned earlier, a crossed butterfly coil together with a single loop coil can be used as independent elements (20) [Fig. 3(d)]. Even though the magnitudes of the coils' sensitivities have the same basic shapes, the phases of their sensitivities are quite different, and thus the two coils can be used effectively in a SENSE reconstruction. A 'saddle train' coil [shown with four elements in Fig. 3(e)] has been proposed to extend the use of crossed coil elements with varying phase into eight-element coil arrays for abdominal and cardiac imaging (44–46).

The contributions of coil phase to spatial encoding were also important in the cardiac array design presented in Ref.35. In part of this design, two planar sets of loop coils were used to reconstruct data in the anterior–posterior direction (perpendicular to the plane of the coil elements). It was found that arranging the coils with a gap between them (rather than overlapping them, as would usually be the case) led to an improved geometry factor for the image planes that were examined. The authors pointed out that while the new positioning of the coils had little effect on the relative magnitudes of the coil sensitivities, the altered spacing did produce variations in coil phase that were useful in the parallel MRI reconstruction. It should be noted that in this study, the coil elements were separated in the left-right direction. A similar study, which examined the SNR performance of a head array composed of circumferentially distributed elements, also found that an increased gap between coil elements led to improved parallel MRI performance (36). Both of these studies suggest that array elements should be separated in directions that are transverse to the main magnetic field direction. By contrast, in the context of conference proceedings, it has been suggested that separation of coil elements in the superior–inferior direction (parallel to the main magnetic field) may not be beneficial (47,48). It should also be noted that each of these studies has approached the question of gapped arrays from the perspective of a fixed number of receiver channels as well as specific array geometries. As more elements are included within arrays and other geometries are explored, the benefit of having gapped arrays may change.

Whatever the specific results, the discussion of coil separation in the previous paragraph provides a significant example of how an optimized coil array for parallel MRI might depart significantly from the geometry generally used for conventional imaging. Another example of using coil elements in non-standard geometries is found in the 'concentric' coil array design (49,50) [Fig.3(f)]. In this type of array, the individual coil elements have increasing numbers of lobes with alternating current directions, and the coils are all placed concentrically on top of each other. The patterns of the current variations help to minimize inductive coupling and noise correlations. The oscillations of magnitude and phase within the coil sensitivities permit the reconstruction of undersampled data, and the concentric arrangement of coil elements allows for spatial encoding in multiple directions. A 'diagonal' array design (51) [Fig. 3(g)] has also been introduced with concentrically placed elements. This array consists of two crossed coils aligned at 45° with respect to the main magnetic field as well as two oblong loop coils. The coil elements are carefully overlapped to reduce the mutual inductance between them. The diagonal array, like the concentric array, was motivated by the desire for multidirectional spatial encoding. Also like the concentric array, it employs an array configuration that is non-standard for conventional imaging, but is very effective for parallel imaging. One final example of an array with concentrically-placed elements consists of a resonant structure tuned so that the signal from three concentric loop coils of varying sizes can be received independently (52). Each of these circular coils is optimized for a different imaging depth. While the authors of this study do not provide specific examples of parallel MRI reconstructions, they

suggest that this type of array might be useful for SENSE imaging.

The concentric array and the diagonal array described above both aim to use coil elements that can participate simultaneously in spatial encoding along several dimensions. The triangle coil array (53) [Fig. 3(h)] is also designed with this flexibility in mind. In one implementation, eight triangular coil elements are arranged around a cylindrical former. The triangular elements provide sensitivity variations both longitudinally and transverse to the cylinder. The decoupled loops from spiral birdcage coils with opposing twists [Fig. 3(i), shown with only one twist direction] have also been proposed for accomplishing multidirectional encoding (54,55). Finally, a group has suggested that simply using two rings of coils, with four simple loops in each ring, might also work well (48).

Specialized coil arrays have been designed for vertical field MRI systems. Because of the orientation of the main magnetic field relative to the surface coils, crossed conductor paths are particularly useful in vertical field systems. A peripheral vascular array has been designed using solenoidal coils together with saddle coils (56,57). A cardiac array has been proposed for a vertical field systems that consists of saddle coils combined with a single large circumferential loop coil (58). In this array design, the loop coil is split into two paths in its anterior portion so that its sensitivity varies in magnitude in the anterior-posterior direction.

As a final example of the use of loop-type coils, parallel MRI has been applied to endovascular imaging. For this purpose, a pair of solenoidal coils with opposing current directions have been used (59).

Arrays based on volume coils

While the majority of coil array designs that have been used for parallel MRI have been based on coil elements with spatially localized sensitivities, so-called volume coils have also been adapted for the task of spatial encoding. This approach was employed in one of the earliest demonstrations of parallel MRI (60). In that example, two coils were used, one with a uniform sensitivity, and the other with a linear gradient sensitivity. Linear combinations of these two coil sensitivities were used to generate successive terms from the Taylor expansion of the complex exponential spatial harmonic.

In another example of volume coils applied to parallel MRI, a set of four independent transmission-line resonators were placed circumferentially around a cylinder (61,62). This arrangement yielded four spatially-selective coil images that could be used in a parallel MRI reconstruction. Similar approaches have been used to design transmit–receive head arrays for four-channel (63) and 15-channel (64) systems for imaging at 7 T and 8 T, respectively. A similar approach based on 'volume lattice arrays' has also been introduced (65). Parallel MRI reconstructions at various acceleration factors using a 32-element transmission line based array have been described (6). A schematic depiction of coil arrays with circumfrentially-arranged linear elements is shown in Fig. 3(j).

Birdcage-type coils can be also adapted for use in spatial encoding. In one approach, a birdcage coil is tuned so that its 'uniform' and 'gradient' modes are degenerate (66) [Fig. 3(k)]. Although the sensitivity patterns for these modes are not spatially localized within particular regions of the field-of-view, they are still distinct enough to reconstruct undersampled data. The use of degenerate modes has also been proposed for a half-volume TEM coil (67).

The conductor arrangements of birdcage-based coils can be tailored to generate highly customized sensitivity patterns. For example, a birdcage coil with specialized conductor placements and capacitor arrangements has been proposed for producing a sinusoidal current pattern across a given field-of-view transverse to the coil axis (15) [Fig. 3(l)]. When used in conjunction with a uniform-sensitivity volume coil, this type of array configuration could, in principle, permit two lines of k-space to be acquired at once with no further processing. Furthermore, a 'spiral' birdcage design (16) [Fig. 3(i)] can be used to produce harmonic sensitivity patterns that are longitudinal to the coil's cylindrical axis. Finally, a current-optimization approach similar to Ref. (15) has been proposed for generating volume-selective sensitivity patterns for use in SENSE imaging (68).

Arrays based on microstrip antennas

Microstrip antennas have also been employed in coil arrays for parallel MRI. The 'planar strip array' (69) and the 'lumped-element planar strip array' (70) have been introduced as methods for generating arrays with densely-spaced elements that are inherently decoupled. A densely-packed array of 64 planar-pair RF coils has also been described (8). When used to acquire data at a shallow depth below the coil elements, this array is capable of acquiring an entire image within a single readout echo, without any need for phase encoding. Looped coil elements based on the microstrip design have been proposed (71), and these elements have also been used as part of a transmit-receive head coil (72).

SPECIAL TOPICS

Arrays of small coils: concerns about depth penetration

As large-scale coil arrays are constructed with increasing numbers of independent elements, and as the individual

elements become smaller in size, there may be some concern that the shallower depth penetration of the individual elements might adversely affect the overall performance of the coil array. It is well known that when a single circular surface coil is used for imaging at a depth z, the maximum SNR is achieved when the surface coil radius is equal to $z/\sqrt{5}$ (73,74). A coil that is smaller than this optimum radius will have a smaller SNR at depth z, and it cannot be used (alone) to 'see' as far into the sample as an optimized coil can. The situation changes, however, when smaller coils are organized into arrays. If a large coil is broken into a set of N adjacent smaller coils occupying the same area, then the superposition principle for electromagnetic fields implies that a simple combination of smaller coils must give the same sensitivity and the same noise as the larger coil. Because the reconstruction specified by eqn (4) [or Ref. (1) for non-parallel MRI] is the optimum linear combination of coils, the combined SNR of the array of small coils must be at least as high as the SNR of the corresponding large coil at arbitrary depth.

The SNR of grid arrays with successively smaller coil elements has been studied theoretically, and it has been shown that, at all depths, the array SNR was computed to be at least as high as the large single-coil SNR (12). For parallel MRI reconstructions, it has been shown in conference proceedings (75) that there is no theoretical disadvantage to using arrays with large numbers of elements to image deep within a sample, although the authors do observe a degradation in SNR experimentally for the smallest array elements, which they suggest may be due to additional circuit-related noise sources. The overall message provided by all of these studies is that, from the perspective of depth penetration, the use of smaller array elements is not necessarily problematic.

There are still several practical challenges that need to be considered as the sizes of array elements are reduced. While a linear combination of small coils can theoretically produce the same sensitivity pattern as a single larger coil, the smaller coils will require more conductor than the single larger one does. These extra conductor paths may bring added noise. As individual coils become smaller, the noise derived from the sample is eventually smaller than the noise derived from the array itself. A linear combination of the 16 elements from a 4×4 grid has been shown to have 5% lower SNR than the equivalent single large loop (76). While detector elements that are coil-noise dominated can still be used for spatial encoding in parallel MRI, they will not be able to provide the same SNR performance as sample-noise dominated coils. If smaller coils are desired, then it is possible to use cooled copper or even superconducting surface coils (77–79). The amount of sample noise is also increased by keeping the coils as close to the sample as possible. Finally, the larger sample resistance that is seen by coils at higher field strengths will allow surface coils for high-field systems to be made much smaller before they become coil-noise dominated.

Adaptive arrays for systems with varying numbers of receivers

With the rapid expansion of the number of available receiver channels on MR systems, coil array designers have sought to develop scalable arrays that work well on systems with varying numbers of receivers. For example, it may be desirable to build a coil array that works well on both eight-channel and four-channel MRI systems. One straightforward solution to this problem has been to combine array elements in certain fixed ratios when fewer receiver channels are available (44–46). Adaptive combinations of coil array elements are also useful when multiple anatomical regions are to be imaged with the same coil array. An eight-channel breast array has been introduced that uses four coil elements around each breast for bilateral imaging but places five elements around a single breast for unilateral imaging (80). Similar approaches have been employed in a neurovascular array (81), a head–neck–spine array (81,82), and a cervical–thoracic–lumbar spine array (83).

In another approach to combining array elements, coil array elements are combined (in hardware) into an alternative basis set that has zero noise correlations between array elements (84–86). The array is called an 'eigencoil'. The desired basis transformation is produced by combining coils according to the Cholesky decomposition of the noise covariance matrix [eqn (5)]. Once the linear combination has been accomplished, the modes with the lowest noise can be selected and connected to the limited receiver channels that are available in a particular system. The 'mode matrix' transformation (87,88) is another adaptive combination of coil array elements that allows coil array elements to be combined in various ways, depending on the number of receivers available and the amount of acceleration that is required. These flexible approaches to coil combination also allow different combinations of coil elements to be chosen based on the selection of different image planes (i.e. with different phase-encode directions) as long as the MR system hardware allows it.

The impact of coil coupling

For a long time, the elimination of inductive coupling has been considered an important part of designing RF coil arrays for MRI. When coils couple inductively, they resonate as a single structure, and it can be very difficult to match the impedance of each element simultaneously to the input impedance of the receiver circuitry. When this match is non-optimal, the preamplifier noise figure can be seriously degraded, leading to an image with a poor SNR.

The development of parallel MRI techniques has led to renewed emphasis on removing coupling and maintaining coil isolation. As mentioned earlier, parallel MRI techniques require a coil array's component-coil sensitivity profiles to be as distinct as possible in order to encode spatial information. When coils couple inductively, they become sensitive to the same regions of the sample, and it has been feared that coupled coils might contain less distinct spatial information than uncoupled coils, yielding lower quality parallel MRI reconstructions.

Several strategies have been proposed for removing the effects of mutual inductance. First, the overlap of adjacent coil elements may be carefully adjusted so that the shared flux between adjacent coils is zero (1). This strategy has the disadvantage that it may restrict the geometrical layouts of the coil elements. Alternatively, capacitive or inductive networks may be built between coils that are able to exactly cancel the mutual inductance between them (89–91). A method for using digital post-processing to emulate the effects of these lumped-element networks has been explored in simulations (92). Additionally, shielded array designs have also been suggested (93). Finally, specialized preamplifiers can be designed that present a large impedance to current flow at the input of each coil (1,94). Because very little current can flow in response to the sample magnetization, the interactions between coil elements are limited.

Recent studies have suggested that if coupling is viewed as a linear transformation of signal and noise, then in principle it should be possible to compensate for the effects of coupling by undoing that linear transformation (40,95). Other authors have suggested that this linear compensation might be complicated by noise from the preamplifiers (96), although the precise impact of this noise source is unclear (97). Phantom-based experiments from Ref. (40) that introduced small amounts of coupling did result in modest SNR changes, but the small magnitude of these changes, taken together with the decoupling strategies described above, suggest that coupling is not likely to be a prohibitive barrier to array design for parallel MRI.

Field strength effects

Significant attention has been given to the design of coil arrays for parallel MRI at magnetic field strengths larger than 1.5 T. It has been shown that the shapes of coil sensitivities change as the field strength increases (98,99). A coil array at a higher field strength might perform differently than a coil array with an identical geometry at a lower field strength (100). In terms of predicting coil sensitivities for coil array design, quasistatic computations are clearly no longer sufficient, and some sort of full-wave electromagnetic approach should be employed (99,101,102). Computational studies have suggested that the increased focusing of RF electromagnetic fields at higher frequencies offer particular benefits for parallel MRI reconstructions (43,103). Specifically, these studies have predicted an enhancement in the ultimate achievable SNR for parallel MRI that is larger than the enhancement that would be expected simply from increased spin polarization. This is a potentially beneficial synergy, as increases in specific absorption rate (SAR) that occur at higher field strengths will make parallel MRI techniques even more critical at those field strengths than they are at 1.5 T. An experimental system has been developed to examine this field strength dependence using a single fixed-field scanner by progressively changing the dielectric properties of the phantom that is used for imaging (100).

Because the wavelength of radiation at high field strengths becomes comparable to the size of the sample, investigators have examined the role of dielectric resonance in parallel MRI. For conventional gradient-encoded imaging, it has been suggested that while dielectric resonances may potentially be supported for human-sized samples and lossless media, these resonances may not be sustainable for samples with physiological conductivities (99,104). In a parallel MRI study, investigators have described changes in parallel MRI performance attributable to dielectric resonance for a salt-free solution, but these changes disappeared for solutions with physiological levels of salinity (105).

Fundamental limits on spatial encoding using coil arrays: implications for coil array design

In view of the vast range of coil array designs that have been explored for parallel MRI, researchers have attempted to determine the ultimate limits on spatial encoding using coil arrays. From the perspective of coil array design, this is an important question, because it helps to distinguish to what extent coil designers are limited by fundamental physical principles and to what extent they are limited by the need to develop more imaginative designs. Broadly speaking, two approaches have been taken to address this question. In each approach, a basis set of coil sensitivities is established, and the optimum-SNR linear combination is determined from this basis set. In the first general approach, the basis set is composed of current paths restricted to a particular surface (e.g. a cylinder), and the optimum SNR found is for coils that reside entirely along that surface (106–108). In the second general approach, the electromagnetic field definitions of the coil sensitivities and noise correlations [eqns (1) and (2)] are used to establish a complete set of basis function sensitivities whose linear combinations are able to represent the sensitivity of any physically realizable coil array (43,103). In principle, these techniques yield the optimal SNR for any attainable coil array, with the array's geometry only restricted by the

requirement that the array remain outside of the sample. In all of these studies, it was found that there are fundamental physical limits to the achievable acceleration using parallel MRI techniques, and these limitations are imposed by the need to satisfy Maxwell's equations. A full discussion of these fundamental limitations is the subject of another article within this issue. For the present discussion, we focus briefly on the potential value of these computational approaches for coil array design.

If a linear combination of coil sensitivities within a basis set is found that optimizes the SNR at a given spatial location, it is theoretically possible to achieve that SNR by constructing a single coil connected to a single receiver with that optimal sensitivity (43,103,108). Therefore, one simple approach to coil array design would be to translate the sensitivity optimizations described in the procedures mentioned above into physical coils. While this procedure is conceptually simple, there are several practical difficulties. These difficulties are different for each of the two classes of coil array optimization.

The advantage of optimization techniques that are based on current sources (106,107) is that these techniques can be used to generate specific current patterns corresponding to coils with optimal SNR. It is unclear, however, whether restricting the conductor elements to a single surface affects the ultimate attainable SNR. This is an important research question because if the optimal SNR were independent of the surface where the detectors were placed, then there would be no need to place coils on the surface of the patient, where they can be cumbersome and uncomfortable. All detector coils could be placed inside the bore of the magnet, where they could be cooled and then connected to the receiver chain in a much simpler process than is currently employed.

The optimization techniques that rely on an electromagnetic field-based sensitivity basis set (43,103) do not require the conductors to be restricted to a single surface, but these techniques have their own challenges when applied to the task of coil array design. Purely sensitivity-based approaches yield optimal coil sensitivity patterns, but they offer no prescriptions for determining the conductor geometry that will be required to produce that sensitivity. It has been pointed out in Ref. (103) that the inverse source problem for the fields in a source-free region is non-unique (109). This non-uniqueness is likely to introduce computational complexities into any algorithm for choosing conductor patterns. Furthermore, the sensitivity patterns that are determined by the field optimizations in Refs (43,103) are only required to satisfy boundary conditions inside of the sample. Nothing is specified about the behavior of the fields outside of the sample. The behavior of the fields on the outside of the sample is important because these exterior fields affect the practicality of any potential coil array. The optimum sensitivity pattern may require current paths that are either infinitely far from or impractically close to the surface of the sample. Large electric and magnetic fields that are generated on the outside of the sample may also lead to inductive and capacitive interactions with surrounding structures.

The conductor-based approaches to SNR optimization and the field-based approaches to SNR optimization have complementary advantages and disadvantages. It should be possible to use the conductor-based approaches in order to generate specific conductor patterns for the optimal coil, and then used the field-based optimization approaches to determine how much SNR has been lost by restricting the coil to a specific surface.

One feature that is common to all of the optimization strategies that have been discussed is that, in principle, different coil sensitivities are required for reconstructing different spatial points for any given acceleration factor. However, it has been noted (103,110) that for Cartesian *k*-space trajectories, the optimum sensitivity for the reconstruction of a particular sample point using parallel MRI can be written as a linear combination of the optimum sensitivities for unaccelerated imaging at all of the potential aliasing points. This result implies that separate coil arrays do not necessarily need to be built for conventional and parallel MRI. However, it is unclear whether this principle is stable for small variations from the optimum. Specifically, if coils are constructed that attain SNR levels within 10% of the optima for fully gradient-encoded images, it is uncertain whether the SNR values for the images reconstructed using parallel MRI will also be within 10% of the optimum. Furthermore, a computed optimum for a particular image plane orientation, FOV, and acceleration factor will not necessarily remain optimal if any of these parameters is changed. Thus, the design of robust tailored arrays for a range of imaging situations is non-trivial.

Practical challenges for large-scale array designs

An important practical consideration when designing coil arrays for high levels of acceleration is the added weight and bulk that accompanies the electronic circuitry and cables that are needed to retrieve the signal from each coil. Smaller, lighter and more efficient signal detection circuitry will clearly be a very important component of these large-scale arrays.

CONCLUSIONS

Parallel MRI techniques have led to new demands on coil array performance. The construction and the arrangement of detector coils must be chosen simultaneously to maximize the SNR of the (unaccelerated) reconstructed data and also to provide spatial information about the magnetization within the sample. These demands have

led to a tremendous expansion of the potential design choices for coil arrays. This rapid expansion has become particularly manifest in the number of available receiver channels on MR systems. There is little doubt that the widening range of parallel MRI applications will lead to array designs that combine and perhaps surpass the strategies that are presented here. It is hoped that this brief review will provide a helpful starting point to understand and to place into context whatever innovations are yet to come.

REFERENCES

1. Roemer PB, Edelstein WA, Hayes CE, Souza SP, Mueller OM. The NMR phased array. *Magn. Reson. Med.* 1990; **16**(2): 192–225.
2. Bankson JA, Griswold MA, Wright SM, Sodickson DK. SMASH imaging with an eight element multiplexed RF coil array. *Magn. Reson. Mater. Phys. Biol. Med.* 2000; **10**: 93–104.
3. Bodurka J, Ledden PJ, van Gelderen P, Chu RX, de Zwart JA, Morris D, Duyn JH. Scalable multichannel MRI data acquisition system. *Magn. Reson. Med.* 2004; **51**(1): 165–171.
4. Zhu Y, Hardy CJ, Sodickson DK, Giaquinto R, Dumoulin CL, Kenwood G, Niendorf T, Lejay H, McKenzie C, Ohliger MA, Rofsky NM. Highly parallel volumetric imaging with a 32-element RF coil array. *Magn. Reson. Med.* 2004; **52**: 878–884.
5. Cline HE, Sodickson DK, Niendorf T, Giaquinto RO. 32-Channel head coil array for highle accelerated parallel imaging applications. In *Proc. 12th Annual Meeting of the International Society for Magnetic Resonance in Medicine*, Kyoto, 2004.
6. Moeller S, Van de Moortele P-F, Adriany G, Snyder CJ, Andersen PM, Strupp JP, Vaughan JT, Ugurbil K. Parallel imaging performance for densely spaced coils in phase arrays at ultra high field strength. In *Proc. 12th Annual Meeting of the International Society for Magnetic Resonance in Medicine*, Kyoto, 2004.
7. Possanzini C, Wantjes M, Verheyen M, Slegt S, Visser F, Jonese A, Overweg J. MRI with a 32-element coil. In *Proc. 12th Annual Meeting of the International Society for Magnetic Resonance in Medicine*, Kyoto, 2004; 1609.
8. McDougall MP, Wright SM, Brown DG. A 64 Channel RF coil array for parallel imaging at 4.7 Tesla. In *11th Annual Meeting of the International Society for Magentic Resonance in Medicine*, Toronto, 2003.
9. Pruessmann KP, Weiger M, Scheidegger MB, Boesiger P. SENSE: Sensitivity encoding for fast MRI. *Magn. Reson. Med.* 1999; **42**(5): 952–962.
10. Sodickson DK, McKenzie CA. A generalized approach to parallel magnetic resonance imaging. *Med. Phys.* 2001; **28**(8): 1629–1643.
11. Pruessmann KP, Weiger M, Bornert P, Boesiger P. Advances in sensitivity encoding with arbitrary *k*-space trajectories. *Magn. Reson. Med.* 2001; **46**(4): 638–651.
12. Wright SM, Wald LM. Theory and application of array coils in MR spectroscopy. *NMR Biomed.* 1997; **10**: 394–410.
13. Sodickson DK, Manning WJ. Simultaneous acquisition of spatial harmonics (SMASH): fast imaging with radiofrequency coil arrays. *Magn. Reson. Med.* 1997; **38**(4): 591–603.
14. Willig J, Brown R, Eagan T, Shvartsman S. *SMASH RF Coil Arrays: Specialized Design Considerations.* In *Proceedings of the 8th Annual Meeting of the International Society for Magnetic Resonance in Medicine*, Denver, CO, 2000; 559.
15. Willig J, Brown R, Eagan T, Shvartsman S. *Perfectly Sinusoidal SMASH Field Shapes from Birdcage Sectors*, In *Proceedings of the 9th Annual Meeting of the International Society for Magnetic Resonance in Medicine*, Glasgow, 2001; 696.
16. Duensing GR, Gotshal U, King S, Huang F. *N*-dimensional orthogonality of volume coils. In *Proc. 10th Annnual Meeting of the International Society for Magnetic Resonance in Medicine*, Honolulu, HI, 2002; 771.
17. Griswold MA, Jakob PM, Nittka M, Goldfarb JW, Haase A. Partially parallel imaging with localized sensitivities (PILS). *Magn. Reson. Med.* 2000; **44**(4): 602–609.
18. Kelton J, Magin RL, Wright SM. An algorithm for rapid image acquisition using multiple receiver coils. In *Proc. 8th Annual Meeting of the Society for Magnetic Resonance in Medicine*, Amsterdam, 1989; 1172.
19. Ra JB, Rim CY. Fast imaging using subencoding data sets from multiple detectors. *Magn. Reson. Med.* 1993; **30**(1): 142–145.
20. Hajnal JV, Larkman DJ, Herlihy DJ. An Array That Exploits Phase for SENSE Imaging. In *Proc. 8th Annual Meeting of the International Society for Magnetic Resonance in Medicine*, Denver, CO, 2000; 1719.
21. Wang Y. Description of parallel imaging in MRI using multiple coils. *Magn. Reson. Med.* 2000; **44**(3): 495–499.
22. Bydder M, Larkman DJ, Hajnal JV. Generalized SMASH imaging. *Magn. Reson. Med.* 2002; **47**(1): 160–170.
23. Yeh EN, McKenzie CA, Lim D, Ohliger MA, Grant AK, Willig J, Rofsky N, Sodickson DK. Parallel Imaging with Augmented Radius in *k*-Space (PARS). In *Proc. 10th Annual Meeting of the International Society for Magnetic Resonance in Medicine*, Honolulu, HI, 2002; 2399.
24. Sodickson DK, Griswold MA, Jakob PM, Edelman RR, Manning WJ. Signal-to-noise ratio and signal-to-noise efficiency in SMASH imaging. *Magn. Reson. Med.* 1999; **41**(5): 1009–1022.
25. McKenzie CA, Ohliger MA, Yeh EN, Price MD, Sodickson DK. Coil-by-coil image reconstruction with SMASH. *Magn. Reson. Med.* 2001; **46**(3): 619–623.
26. Griswold MA, Jakob PM, Heidemann RM, Nittka M, Jellus V, Wang JM, Kiefer B, Haase A. Generalized autocalibrating partially parallel acquisitions (GRAPPA). *Magn. Reson. Med.* 2002; **47**(6): 1202–1210.
27. Yeh EN, McKenzie C, Grant AK, Ohliger MA, Willig-Onwuachi JD, Sodickson DK. Generalized noise analysis for magnitude image combinations in parallel MRI. In *Proc. 11th Annual Meeting of the International Society for Magnetic Resonance in Medicine*, Toronto, 2003; 21.
28. Bankson JA, Wright SM. Simulation-based investigation of partially parallel imaging with a linear array at high accelerations. *Magn. Reson. Med.* 2002; **47**(4): 777–786.
29. Hoult DI, Richards RE. The signal-to-noise ratio of the nuclear magnetic resonance experiment. *J. Magn. Reson.* 1976; **24**: 71–85.
30. Vesselle H, Collin RE. The signal-to-noise ratio of nuclear magnetic resonance surface coils and application to a lossy dielectric cylinder model—part I: theory. *IEEE Trans. Biomed. Engng* 1995; **42**(5): 497–505.
31. Haake EM, Brown RW, Thompson MR, Venkatesan R. *Magnetic Resonance Imaging: Physical Principles and Sequence Design.* Wiley-Liss: New York, 1999.
32. Hoult DI. The principle of reciprocity in signal strength calculations—a mathematical guide. *Conc. Magn. Reson.* 2000; **12**(4): 173–187.
33. Nyquist H. Thermal agitation of electric charge in conductors. *Phys. Rev.* 1928; **32**: 110–113.
34. Jackson JD. *Classical Electrodyamics*. Wiley: New York, 1999.
35. Weiger M, Pruessmann KP, Leussler C, Roschmann P, Boesiger P. Specific coil design for SENSE: a six-element cardiac array. *Magn. Reson. Med.* 2001; **45**(3): 495–504.
36. de Zwart JA, Ledden PJ, Kellman P, van Gelderen P, Duyn JH. Design of a SENSE-optimized high-sensitivity MRI receive coil for brain imaging. *Magn. Reson. Med.* 2002; **47**(6): 1218–1227.
37. de Zwart JA, Ledden PJ, van Gelderen P, Bodurka J, Chu RX, Duyn JH. Signal-to-noise ratio and parallel imaging performance of a 16-channel receive-only brain coil array at 3.0 Tesla. *Magn. Reson. Med.* 2004; **51**(1): 22–26.
38. Constantinides CD, Atalar E, McVeigh ER. Signal-to-noise measurements in magnitude images from NMR phased arrays. *Magn. Reson. Med.* 1997; **38**(5): 852–857.
39. Sodickson DK, Griswold MA, Jakob PM, Edelman RR, Manning WJ. Signal-to-noise ratio and signal-to-noise efficiency in SMASH imaging. *Magn. Reson. Med.* 1999; **41**(5): 1009–1022.
40. Ohliger MA, Ledden P, McKenzie C, Sodickson DK. The effects of inductive coupling on parallel MR image reconstructions. *Magn. Reson. Med.* 2004; **52**(3): 628–639.

41. Hardy CJ, Darrow RD, Saranathan M, Giaquinto R, Zhu Y, Dumoulin CL, Bottomley PA. Large field-of-view real-time MRI with a 32-channel system. *Magn. Reson. Med.* 2004; **52**: 878–884.
42. Weiger M, Pruessmann KP, Boesiger P. 2D SENSE for faster 3D MRI. *Magn. Reson. Mater. Phys. Biol. Med.* 2002; **14**(1): 10–19.
43. Ohliger MA, Grant AK, Sodickson DK. Ultimate intrinsic signal-to-noise ratio for parallel MRI: Electromagnetic field considerations. *Magn. Reson. Med.* 2003; **50**(5): 1018–1030.
44. Spence DK, Fujita H. A new coil array for SENSE imaging with four and eight receivers. In *Proc. 10th Annual Meeting of the International Society for Magnetic Resonance in Medicine*, Honolulu, HI, 2002.
45. Fujita H, Spence DK. A novel 8-channel 'saddle-train' array coil for cardiac SENSE Imaging at 1.5 T. In *Proc. 10th Annual Meeting of the International Society for Magnetic Resonance in Medicine*, Honolulu, HI, 2002.
46. Fujita H, Spence DK. A Novel 8-channel 'saddle-train' array coil for abdominal SENSE Imaging at 1.5 T. In *Proc. 10th Annual Meeting of the International Society for Magnetic Resonance in Medicine*, Honolulu, HI, 2002.
47. Klinge JHA, Davis SC, Gangakhedkar DD, Lindsey SA, Blawat L. An 8-channel cardiac SENSE array. In *Proc. 10th Annual Meeting of the International Society for Magnetic Resonance in Medicine*, 2002.
48. Iwadate Y, Boskamp E, Nabetani A, Tsukamoto T. Design of an 8-channel head coil for SENSE acceleration in 2 directions. In *Proc. 12th Annual Meeting of the International Society for Magnetic Resonance in Medicine*, Kyoto, 2004; 1613.
49. Ohliger MA, Greenman R, McKenzie CA, Sodickson DK. Concentric coil arrays for spatial encoding in parallel MRI. In *Proc. 9th Annual Meeting of the International Society for Magnetic Resonance in Medicine*, Glasgow, 2001.
50. Ohliger MA, Greenman R, McKenzie CA, Wiggins G, Giaquinto RO, Sodickson DK. Concentric coil arrays for multidimensional spatial encoding in cardiac parallel MRI. In *Proc. 12th Annual Meeting of the International Society for Magnetic Resonance in Medicine*, Kyoto, 2004.
51. Chan PH, Michael K, Anderson B. Diagonal-arranged quadrature coil arrays for 3D SENSE imaging. In *Proc. 12th Annual Meeting of the International Society for Magnetic Resonance in Medicine*, Kyoto, 2004; 2382.
52. Luessler C, Mazurkewitz P, Bornert P. Intrinsic hybrid surface coil array for improved SNR in cardiac MRI. In *Proc. 10th Annual Meeting of the International Society for Magnetic Resonance in Medicine*, Honolulu, HI, 2002.
53. Seeber DA, Pikelja V, Jevtic I. New RF coil topology for high performance SENSE in 3D. In *Proc. 11th Annual Meeting of the International Society for Magnetic Resonance in Medicine*, Toronto, 2003; 465.
54. Mueller MF, Griswold MA, Haase A, Jakob PM. Design considerations for volumetric arrays with many elements for massively parallel MRI. In *Proc. 11th Annual Meeting of the International Society for Magnetic Resonance in Medicine*, Toronto, 2003; 2340.
55. Mueller M, Breuer F, Blaimer M, Heidemann R, Webb A, Griswold MA, Jakob PM. 8 channel double spiral head array coil for enhanced 3D parallel MRI at 1.5T. In *Proc. 12th Annual Meeting of the International Society for Magnetic Resonance in Medicine*, Kyoto, 2004.
56. Su SY, Zou MXM, Murphy-Boesch J. Solenoidal array coils. *Magn. Reson. Med.* 2002; **47**(4): 794–799.
57. Su S, Robb F, Guan Y, Zhao S. A novel 15-element SENS-compatible vertical field PV array coil. In *Proc. 12th Annual Meeting of the International Society for Magnetic Resonance in Medicine*, Kyoto, 2004.
58. Feng L, Chen V, Yang YL. The SENSE cardiac coil for 4-channel vertical field MRI systems. In *Proc. 12th Annual Meeting of the International Society for Magnetic Resonance in Medicine*, Kyoto, 2004; 1600.
59. Hillenbrand CM, Wong EY, Griswold MA, Zhang S, Rafie S, Lewin JS, Durek JL. Intravascular parallel imaging: a feasibility study. In *Proc. 12th Annual Meeting of the International Society for Magnetic Resonance in Medicine*, Kyoto, 2004; 376.
60. Carlson JW, Minemura T. Imaging time reduction through multiple receiver coil data acquisition and image-reconstruction. *Magn. Reson. Med.* 1993; **29**(5): 681–688.
61. Lin F-H, Ledden PJ, Kwong KK, Belliveau JW, Wald LL. SENSE imaging using a transmission line volume phased array. In *Proc. 9th Annual Meeting of the International Society for Magnetic Resonance in Medicine*, Glasgow, 2001.
62. Tropp J, Sodickson DK, Ohliger MA. Feasibility of a TEM surface array for parallel imaging. In *Proc. 10th Annual Meeting of the International Society for Magnetic Resonance in Medicine*, Honolulu, HI, USA, 2002; 856.
63. Abduljalil AM, Schmalbrock P, Gilbert R, Chakeres DW. SENSE imaging with multi-port TEM coils at ultra high field. In *Proc. 12th Annual Meeting of the International Society for Magnetic Resonance in Medicine*, Kyoto, 2004; 473.
64. Adriany G, Van de Moortele P-F, Andersen PM, Strupp JP, Ritter JB, Snyder CJ, Moeller S, Vaughan JT, Ugurbil K. An elliptical open-face transceive array for ultra high field parallel imaging and fMRI applications. In *Proc. 12th Annual Meeting of the International Society for Magnetic Resonance in Medicine*, Kyoto, 2004; 1604.
65. Lee RF, Boskamp EB, Giaquinto RO, Ohliger MA, Sodickson DK. A 16-channel transmit/receive volume lattice array (VLA) for high acceleration in parallel imaging. In *Proc. 11th Annual Meeting of the International Society for Magnetic Resonance in Medicine*, Toronto, 2003; 467.
66. Lin FH, Kwong KK, Huang IJ, Belliveau JW, Wald LL. Degenerate mode birdcage volume coil for sensitivity-encoded imaging. *Magn. Reson. Med.* 2003; **50**(5): 1107–1111.
67. Avdievich NI, Peshovsky A, Kennan RO, Hetherington HP. SENSE imaging with quadrature half-volume TEM coil at 4 T. In *Proc. 12th Annual Meeting of the International Society for Magnetic Resonance in Medicine*, Kyoto, 2004; 1590.
68. Eagan TP, Willig-Onwuachi JD, Shvartsman SM, Cheng YCN, Brown DG. The SENSE-cage: a half-birdcage volume coil. In *Proc. 12th Annual Meeting of the International Society for Magnetic Resonance in Medicine*, Kyoto, 2004; 1606.
69. Lee RF, Westgate CR, Weiss RG, Newman DC, Bottomley PA. Planar strip array (PSA) for MRI. *Magn. Reson. Med.* 2001; **45**(4): 673–683.
70. Lee RF, Hardy CJ, Sodickson DK, Bottomley PA. Lumped-element planar strip array (LPSA) for parallel MRI. *Magn. Reson. Med.* 2004; **51**(1): 172–183.
71. Wu B, Qu P, Wang C, Shen GX. A new array design using tunable loop microstrip (TLM) coil. In *Proc. 12th Annual Meeting of the International Society for Magnetic Resonance in Medicine*, Kyoto, 2004; 1576.
72. Adriany G, Van de Moortele P, Wiesinger F, Andersen P, Strupp J, Zhang X, Snyder CJ, Chen W, Pruessmann K, Boesiger P, Vaughan JT, Ugarbil K. Transcieve stripline arrays for ultra high field parallel imaging applications. In *Proc. 11th Annual Meeting of the International Society for Magnetic Resonance in Medicine*, Toronto, 2003; 474.
73. Roemer PB, Edelstein WA. Ultimate sensitivity limits of surface coils. In *Proc. 6th Annual Meeting of the Society for Magnetic Resonance in Medicine*, New York, 1987; 410.
74. Wang J, Reykowski A, Dickas J. Calculation of the signal-to-noise ratio for simple surface coils and arrays of coils. *IEEE Trans. Biomed. Engng* 1995; **42**(9): 908–917.
75. Sodickson DK, Lee RF, Giaquinto RO, Collins CM, McKenzie CA, Ohliger MA, Grant AK, Willig-Onwuachi JD, Yeh EN, Kressel HY. Depth penetration of RF coil arrays for sequential and parallel MR imaging. In *Proc. ISMRM 11th Annual Meeting*, Toronto, 2003; 469.
76. Duensing GR, Akao J, Saylor C, Molyneaux D. Conductor losses in many channel RF coil arrays. In *Proc. 12th Annual Meeting of the International Society for Magnetic Resonance in Medicine*, Kyoto, 2004; 1583.
77. Wosik J, Xie LM, Nesteruk K, Xue L, Bankson JA, Hazle JD. Superconducting single and phased-array probes for clinical and research MRI. *IEEE Trans. Applied Superconductivity* 2003; **13**(2): 1050–1055.
78. Kwok WE, You ZG, Zhong J. Improved high resolution imaging with 4-element liquid nitrogen phased array coil and VD-AUTO-SMASH at 1.5T. In *Proc. 11th Annual Meeting of the Inter-*

national Society for Magnetic Resonance in Medicine, Toronto, 2003; 430.
79. De Zanche N, Leussler C, Mandelkow H, Pruessmann KP. A 6-element array for parallel wrist imaging at 3 Tesla. In *Proc. 12th Annual Meeting of the International Society for Magnetic Resonance in Medicine*, Kyoto, 2004; 1591.
80. Qu K, Chan PH, Zheng T, Maier C, Murphy J. A 10-element medial and lateral accessible breast coil array optimized for parallel imaging. In *Proc. 12th Annual Meeting of the International Society for Magnetic Resonance in Medicine*, Kyoto, 2004; 1597.
81. Okamoto K, Takagi M, Yasihara Y, Fujita H, Zhang Y, Payton C, Donofrio M. A novel 'smart' neurovascular array coil system for parallel imaging. In *Proc. 12th Annual Meeting of the International Society for Magnetic Resonance in Medicine*, Kyoto, 2004; 1595.
82. Chan PH, Scott T, Phelan K, Anderson B, Petropoulos L. A 21-channel High performance combo head-neck-spine-cardiac coil for 3D parallel imaging applications. In *Proc. 12th Annual Meeting of the International Society for Magnetic Resonance in Medicine*, Kyoto , 2004.
83. Feng L, Chen V, Lakshmanan K, Yang YL. The SENSE CTL coil for 3 T 8-channel MRI Systems. In *Proc. 12th Annual Meeting of the International Society for Magnetic Resonance in Medicine*, Kyoto, 2004; 2634.
84. Varosi SM, King SB, Duensing GR. A hardware combiner to achieve 'optimal' SNR using sum-of-squares reconstruction. In *Proc. 10th Annual Meeting of the International Society for Magnetic Resonance in Medicine*, Honolulu, HI, 2002.
85. King SB, Varosi SM, Huang F, Duensing GR. The MRI eigencoil: 2 *N*-channel SNR with *N*-receivers. In *Proc. 11th Annual Meeting of the International Society for Magnetic Resonance in Medicine*, Toronto, 2003; 712.
86. Gotshal U, Duensing GR, Saylor CA, Akao J, Huang F, Holland A, Molyneaux DA. The Linear Eigencoil. In *Proc. 12th Annual Meeting of the International Society for Magnetic Resonance in Medicine*, Kyoto, 2004.
87. Reykowski A, Blasche M. Mode matrix—a generalized signal combiner for parallel imaging arrays. In *Proc. 12th Annual Meeting of the International Society for Magnetic Resonance in Medicine*, Kyoto, 2004; 1587.
88. Reykowski A, Hemmerlein M, Wolf S. A novel head/neck coil design using matrix clusters and mode combiners. In *Proc. 12th Annual Meeting of the International Society for Magnetic Resonance in Medicine*, Kyoto, 2004.
89. Jevtic J. *Ladder Networks for Capacitive Decoupling in Phased-Array Coils*. Glasgow, 2001; **17**: 2393.
90. Lee RF, Giaquinto RO, Hardy CJ. Coupling and decoupling theory and its application to the MRI phased array. *Magn. Reson. Med.* 2002; **48**(1): 203–213.
91. Jevtic J, Pikelja V, Menon A, Seeber D, Tatum N. Design Guidelines for the Capacitive Decoupling Networks. In *Proc. 11th Annual Meeting of the International Society for Magnetic Resonance in Medicine*, Toronto, 2003; 428.
92. Song XY, Wang WD, Zhang BD, Lei M, Bao SL. Digitalization decoupling method and its application to the phased array in MRI. *Prog. Nat. Sci.* 2003; **13**(9): 683–689.
93. Wang J-X, Plewes DB. Decoupling of strongly coupled MRI surface coils using virtual-shield method. In *Proc. 12th Annual Meeting of the International Society for Magnetic Resonance in Medicine*, Kyoto, 2004; 1584.
94. Ledden P, Inati S. Four channel preamplifier decoupled phased array for brain imaging at 1.5 T. In *Proc. 9th Annual Meeting of the International Society for Magnetic Resonance in Medicine*, Glasgow, 2001; 1117.
95. Pruessmann K, Weiger M, Wiesinger F, Boesiger P. An investigation into the role of coil coupling in parallel imaging. In *Proc. ISMRM 10th Annual Meeting*, Honolulu, HI, 2002; 196.
96. Duensing GR, Brooker HR, Fitzsimmons JR. Maximizing signal-to-noise ratio in the presence of coil coupling. *J. Magn. Reson. Ser. B* 1996; **111**(3): 230–235.
97. Scott G. Preamplifier noise input coupling for phased arrays. In *Proc. ISMRM 10th Annual Meeting*, Honolulu, 2002; 894.
98. Ledden P, Duyn JH. Ultra-high frequency array performance: predicted effects of dielectric resonance. In *Proc. ISMRM 10th Annual Meeting*, Honolulu, HI, 2002; 324.
99. Yang QX, Wang JH, Zhang XL, Collins CM, Smith MB, Liu HY, Zhu XH, Vaughan JT, Ugurbil K, Chen W. Analysis of wave behavior in lossy dielectric samples at high field. *Magn. Reson. Med.* 2002; **47**(5): 982–989.
100. Wiesinger F, Van de Moortele P-F, Adriany G, De Zanche N, Ugurbil K, Pruessmann K. Parallel imaging performance as a function of field strength—an experimental investigation using electromagnetic scaling. *Magn. Reson. Med.* 2004; **5**: 953–964.
101. Wright SM. Full-wave analysis of planar radiofrequency coils and coil arrays with assumed current distribution. *Conc. Magn. Reson.* 2002; **15**(1): 2–14.
102. Wright SM. 2D full-wave modeling of SENSE coil geometry factors at high field. In *Proc. 10th Annual Meeting of the International Society for Magnetic Resonance in Medicine*, Honolulu, HI, 2002.
103. Wiesinger F, Boesiger P, Pruessmann KP. Electrodynamics and ultimate SNR in parallel MR imaging. *Magn. Reson. Med.* 2004; **52**: 376–390.
104. Hoult DI. Sensitivity and power deposition in a high-field imaging experiment. *J. Magn. Reson. Imag.* 2000; **12**(1): 46–67.
105. Wiesinger F, Van de Moortele P-F, Adriany G, De Zanche N, Snyder C, Vaughan T, Ugurbil K, Pruessmann K. An investigation into the role of dielectric resonance in parallel imaging. In *Proc. 12th Annual Meeting of the International Society of Magnetic Resonance in Medicine*, Kyoto, 2004.
106. Reykowski A, Schnell W, Wang J. Simulation of SNR limit for SENSE related reconstruction techniques. In *Proc. ISMRM 10th Annual Meeting*, Honolulu, HI, 2002; 2385.
107. Griswold MA, Lanz T, Haase A, Jakob PM. *A Brute-Force Estimation of the SNR Limits of Sensitivity Encoding in a Cylindrical Geometry.* In *Proceedings of the 10th Annual Meeting of the International Society for Magnetic Resonance in Medicine*, Honolulu, 2002; 2385.
108. Mazurkewitz P, Schulz V, Singer H. Simulations with optimized SENSE-coil arrays. In *Proc. 11th Annual Meeting of the International Society for Magnetic Resonance in Medicine*, Toronto, 2003.
109. Bleistein N, Cohen JK. Nonuniqueness in the inverse source problem in acoustics and electromagnetics. *J. Math. Phys.* 1976; **18**(2): 194–201.
110. Reykowski A. How to calculate the SNR limit of SENSE related reconstruction techniques. In *Proc. 10th Annual Meeting of the International Society for Magnetic Resonance in Medicine*, Honolulu, HI, 2002; 905.
111. Morris HD, Seeber D. Multi-direction SENSE imaging using a head coil based on triangular elements with a standard clinical scanner. In *Proc. 12th Annual Meeting of the International Society for Magnetic Resonance in Medicine*, Kyoto, 2004; 1598.

